Microstructures of phases in indented silicon: A high resolution characterization

I. Zarudi
School of Aerospace, Mechanical and Mechatronic Engineering, The University of Sydney, NSW 2006, Australia

J. Zou
Australian Key Centre for Microscopy and Microanalysis and Electron Microscope Unit, The University of Sydney, NSW 2006, Australia

L. C. Zhang[a)]
School of Aerospace, Mechanical and Mechatronic Engineering, The University of Sydney, NSW 2006, Australia

(Received 15 July 2002; accepted 5 December 2002)

This letter investigates the structural changes in monocrystalline silicon caused by microindentation with the aid of the high-resolution transmission electron microscopy. It shows that the transformation zone is amorphous when the maximum indentation load, $P_{\max}$, is low, but a crystalline phase of high-pressure R8/BC8 can appear when $P_{\max}$ increases. The nanodeformation of the pristine silicon outside the transformation zone proceeds with the mechanical bending and distortion of the crystalline planes. Certain extent of plastic deformation took place due to dislocation slipping. The results seem to indicate that the shear stress component played an important role in the deformation of the transformation zone. © *2003 American Institute of Physics.* [DOI: 10.1063/1.1544429]

Microindentation has been an effective technique for understanding the microstructures and defects in silicon caused by micro/nanomachining. Details of the microstructure in the transformation zone after a single or a multiple indentation have been carefully studied by various methods, the Raman spectroscopy,[1–3] scanning/atomic force microscopy[4–7] and the transmission electron microscopy (TEM) on both the plan-view[4] and cross-section[7–12] specimens.

It was reported[9,13–16] that during loading, a phase transformation occurred, giving rise to the β-Sn phase. The event was predicted theoretically[14,17] and confirmed experimentally by a drop in contact resistance.[13] A further phase transformation was identified during unloading, in which the β-Sn phase transferred to either the amorphous or the high-pressure R8/BC8 phase or a mixture of them.[9,10] In addition, it was concluded that the phases were metastable[18] and the microstructure of the transformed material was dependent on the maximum indentation load[9] and the number of loading/unloading increments.[11] Theoretical modeling using molecular dynamics simulations demonstrated that a transformation from β-Sn phase to amorphous could also take place even when the indenter's radius was a few nanometers.[17,19] On the other hand, it was suggested that the amorphization of silicon in indentation with Vickers indenter proceeded directly from its diamond structure due to high defect concentration[12] or dislocation activity.[20] Nevertheless, there are still some controversial opinions on the sequence of the transformations and the nature of the phases. A few studies by the high-resolution transmission electron microscopy (HRTEM) have been carried out to investigate the indented materials. Wu *et al.*[12] analyzed the structure of monocrystalline silicon after Vickers indentation. However, the effect of the maximum indentation load remains unclear.

This letter reports the HRTEM characterization results of monocrystalline silicon after the microindentation under various maximum indentation loads, $P_{\max}$. Analysis of the atomistic structure of the subsurface region, including the phase transformation zone, the distorted pristine silicon and the transitional region between them, will be used to attain an insight into the phase transformation and plastic deformation.

The indentation tests on the (100) Si surfaces with $P_{\max}=30$ and 90 mN were performed using an Ultra-Micro-Indentation-System-2000 (UMIS-2000) with a spherical indenter having a nominal radius of 5 μm. The average loading–unloading rate was 3 mN/s. Conventional TEM studies were carried out in a Philips CM12 transmission electron microscope, operating at 120 kV and the HRTEM investigation was performed in a JEOL JEM-3000F transmission electron microscope, operating at 300 kV.

The $\langle 110 \rangle$ cross-section TEM specimens were prepared by an improved technique using a tripod.[9] In the preparation, the material removal was continuously monitored and the sample position with respect to the tripod was adjusted during the mechanical thinning. Finally, the ion-beam thinning was carried out to provide a sufficiently thin area for the TEM investigations.

Figure 1 shows the diffraction contrast images, demonstrating the morphology and microstructure of the transformation zone with different $P_{\max}$. Diffraction patterns were inserted to indicate the crystallinity inside the transformation zone. Figure 1(a) presents the amorphous phase with $P_{\max}$

a)Electronic mail: zhang@mech.eng.usyd.edu.au

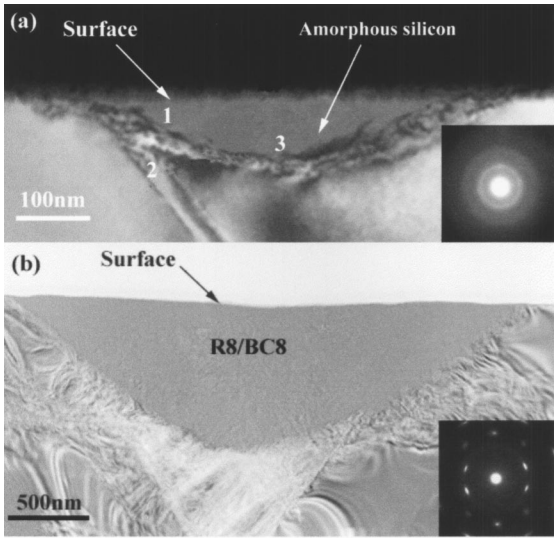

FIG. 1. Microstructure of the transformation zone with different P_{max} (diffraction patterns of the transformation zones are inserted): (a) a dark-field TEM image taken from the $P_{max}=30$ mN specimen; (b) A bright-field TEM image taken from the $P_{max}=90$ mN specimen.

$=30$ mN and Fig. 1(b) shows the crystalline phase with $P_{max}=90$ mN.

Figure 2 is a HRTEM image taken from the transformation zone in the specimen indented with $P_{max}=90$ mN. Polycrystals are clearly seen with sizes varying between 3 and 15 nm. The single diffraction pattern with arcs [see Fig. 1(b)] indicates that polycrystals have roughly the same orientation, suggesting a coherent nucleation and growth mechanism. This implies that although the nucleation processes of individual crystals are independent, the nuclei must be formed in a certain array. In fact, the disorientation between these polycrystals can be measured from the width of these arcs. The maximum disorientation was determined to be 12°. In addition, the disorientation has been reflected in the HRTEM image. For example, a disorientation of three degrees can be identified between crystals C1 and C2 in Fig. 2.

The electron diffraction investigation suggests that the crystals in the transformation zone are a mixture of two metastable phases, R8 and BC8.[21] In addition, the formation of the R8/BC8 phase at different unloading conditions could cause a change in the orientation of the crystalline particles in the azimuth direction, leading to a follow-on disorientation of polycrystals.

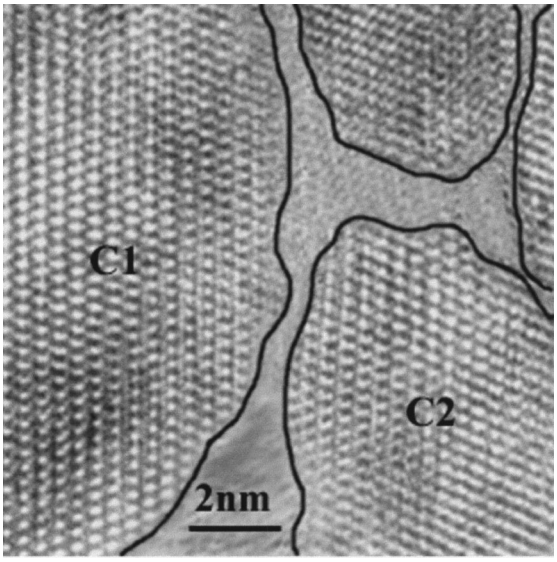

FIG. 2. HRTEM image of the $P_{max}=90$ mN specimen showing polycrystals inside the transformation zone.

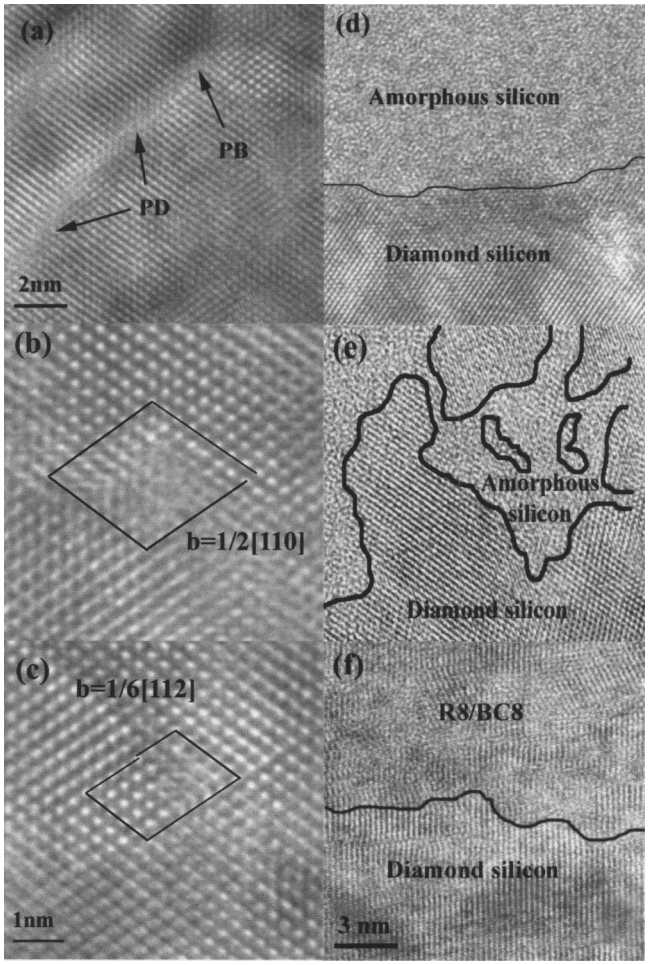

FIG. 3. HRTEM images (a)–(c): details of the plastic deformation in the pristine silicon near the transformation region: (a) plane bending (PB) and plane distortion (PD); (b) a perfect 60° dislocation; and (c) lattice shifting; (d) to (f): boundaries between the transformation zone and the pristine silicon: (d) taken from region 3 of Fig. 1(a); (e) taken from region 1 of Fig. 1(a); and 1(f) at the boundary in Fig. 1(b).

The deformation of pristine silicon in the vicinity of the transformation zone was also studied. Figure 3 is an example at $P_{max}=30$ mN in area 2 as marked in Fig. 1(a). Figure 3(a) illustrates the lattice distortion in two ways: (1) the lattice bending reflected by the nonuniform lattice image, and (2) the internal strain demonstrated by the nonuniform background. Figure 3(b) shows a 60° perfect dislocations with Burgers vector of $1/2\langle 110\rangle$. Here the 60° means the angle between the dislocation line and its Burgers vector. It should be noted that only the edge component of the dislocations with their dislocation lines parallel to the viewing direction can be determined by HRTEM ($\langle 110\rangle$ direction in this case). Therefore, the dislocations observed are gliding dislocations and are not necessarily 60° as long as they remain in their glide plane. They are mobile and endorse plastic deformation. Figure 3(c) shows the lattice shifting (as marked) which can be caused by several mechanisms. However, incidence

of an extra half plane on one side of the lattice shifting suggests that it is due to the dissociation of a gliding dislocation, possibly caused by a stacking fault associated with a Shockley partial dislocation (Burgers vector: $1/6\langle 112\rangle$). Since only gliding dislocations (perfect and dissociated) were observed, it seems to conclude that the shear stresses on the {111} slip planes are the driving force for the formation of these dislocations. These observations align well with the recent theoretical investigations[19,22] which proposed that deviatoric stresses play an important role in the phase transformation of silicon.

Figure 1 shows that under light indentation (e.g., $P_{\max}=30$ mN), the dislocations just started to slip, while under heavy indentation (e.g., $P_{\max}=90$ mN), multiple slipping occurred. Hence, a certain extent of plastic deformation was caused by dislocations slipping on their glide planes.

We now investigate the boundary between the transformation zone and the pristine silicon. The boundary structure is crucial for determining the mechanical properties of the indentation-affected material, as the boundary can be a source of additional imperfections, defects and stress concentrators. Subsequently its structure should be carefully examined.

Figure 3(d) is a HRTEM image taken from the material in region 3 of Fig. 1(a), showing a smooth boundary. Figure 3(e) is a typical one from region 1 of Fig. 1(a), indicating a rough boundary. It is interesting to note that diamond-structured crystals exist inside the amorphous phase, which indicates that more amorphization took place in region 3.

Some recent elastic–plastic analyses by means of the finite element method[22,23] and molecular dynamics simulations[24] explored the distributions of shear and hydrostatic stresses when phase transformations occurred in monocrystalline silicon under indentation. The results showed that the magnitude of the maximum shear stress in the central part of the boundary (near the indentation axis) was higher. The hydrostatic stress, however, was higher at the surface. This seems to indicate that the endorsement of the amorphous phase in region 3 is related to the level of the maximum shear stress.

Figure 3(f) shows a typical boundary between the transformation zone and the diamond silicon in a specimen indented with $P_{\max}=90$ mN. Although the boundary is not as flat as that at the bottom region when $P_{\max}=30$ mN, it can be claimed fairly as a smooth boundary.

Wu *et al.*[12] suggested that amorphous silicon can be produced directly from diamond-Si in the test with a Vickers indenter. If it were true in our case with the spherical indenter, we should expect to see amorphous in the transformation zone with all the $P_{\max}$. However, it is not the case when $P_{\max}=90$ mN. This seems to suggest that the stress field generated by the spherical indenter promotes multiple phase transformations.

The discussion above has shown that shear stresses endorse the amorphous phase transformation. Its role is also pronounced in the deformation of the pristine silicon, because the formation of the gliding dislocations on their slip systems could be realized only by shear stresses. Thus overall, the shear stresses play an important role in both the phase transformation and the deformation of the pristine silicon outside the transformation zone.

In short, the deformation behavior of monocrystalline silicon under the microindentation process can be summarized as follows:

(1) Most of the deformed zone underwent phase transformations. The structure of the material in the zone was amorphous when the maximum indentation load $P_{\max}$ was low but converged to the crystalline high-pressure R8/BC8 phases when $P_{\max}$ increased.

(2) The nanocrystals of the R8/BC8 phases under the high $P_{\max}$ showed a coherent nucleation and growth mechanism with azimuth disorientation up to 12°.

(3) The nanodeformation of pristine silicon outside the transformation zone proceeded with mechanical bending and distortion of crystalline planes accompanied by the formation of gliding dislocations.

(4) The boundary between amorphous and pristine silicon was rather smooth at the bottom of the transformation zone but became rougher near the sample surface.

(5) The shear stress component played an important role in both the phase transformation and deformation of pristine silicon.

The authors wish to thank the Australian Research Council for continuing support of this project.

[1] Y. G. Gogotsi, V. Domnich, S. N. Dub, A. Kailer, and K. G. Nikel, J. Mater. Res. **15**, 871 (2000).
[2] A. Kailer, K. G. Nickel, and Y. G. Gogotsi, J. Raman Spectrosc. **30**, 939 (1999).
[3] V. Domnich, Y. G. Gogotsi, and S. N. Dub, Appl. Phys. Lett. **76**, 2214 (2000).
[4] D. L. Callagan and J. C. Morris, J. Mater. Res. **7**, 1614 (1992).
[5] G. M. Pharr, W. C. Oliver, and D. C. Harding, J. Mater. Res. **6**, 1129 (1991).
[6] D. R. Clarke, M. C. Kroll, P. D. Kirchner, and R. F. Cook, Phys. Rev. Lett. **60**, 2156 (1988).
[7] L. C. Zhang and I. Zarudi, Int. J. Mech. Sci. **43**, 1985 (2001).
[8] I. Zarudi and L. C. Zhang, in *Abrasive Technology* (World Scientific, Singapore, 1999), p. 437.
[9] I. Zarudi and L. C. Zhang, Tribol. Int. **32**, 701 (1999).
[10] J. E. Bradby, J. S. Williams, M. V. Wong-Leung, M. V. Swain, and P. Munroe, J. Mater. Res. **16**, 1500 (2001).
[11] J. E. Bradby, J. S. Williams, M. V. Wong-Leung, M. V. Swain, and P. Manroe, Appl. Phys. Lett. **77**, 3749 (2000).
[12] Y. Q. Wu, X. Y. Yang, and Y. B. Xu, Acta Mater. **47**, 2431 (1999).
[13] I. V. Gridneva, Y. V. Milman, and V. I. Trefilov, Phys. Status Solidi **14**, 177 (1972).
[14] W. C. D. Cheong and L. C. Zhang, Nanotechnology **11**, 173 (2000).
[15] A. B. Mann, D. v. Heerden, J. B. Pethica, and T. P. Weihs, J. Mater. Res. **15**, 1754 (2000).
[16] L. C. Zhang and I. Zarudi, Key Eng. Mater. **177–180**, 121 (2000).
[17] W. C. D. Cheong and L. C. Zhang, Mater. Sci. Lett. **19**, 439 (2000).
[18] J. Crain, G. J. Ackland, J. R. Maclean, R. O. Piltz, P. D. Hatton, and G. S. Pawley, Phys. Rev. B **50**, 13043 (1994).
[19] L. C. Zhang and H. Tanaka, JSME Int. J. Ser. A: Solid Mech. Mater. Eng. **14**, 546 (1999).
[20] M. Tachi, S. Suprijadi, S. Arai, and H. Saka, Philos. Mag. **82**, 133 (2002).
[21] I. Zarudi, J. Zou, and L. C. Zhang (unpublished).
[22] T. Vodenitcharova, L. C. Zhang, and T. X. Yu, Key Eng. Mater. **233–236**, 621 (2003).
[23] T. Vodenitcharova and L. C. Zhang (unpublished).
[24] W. C. D. Cheong and L. C. Zhang, Key Eng. Mater. **233–236**, 603 (2003).